Titania with Alkaline Treated Graphitic Carbon Nitride (g-C_3N_4) to Improve Photocatalysis Properties

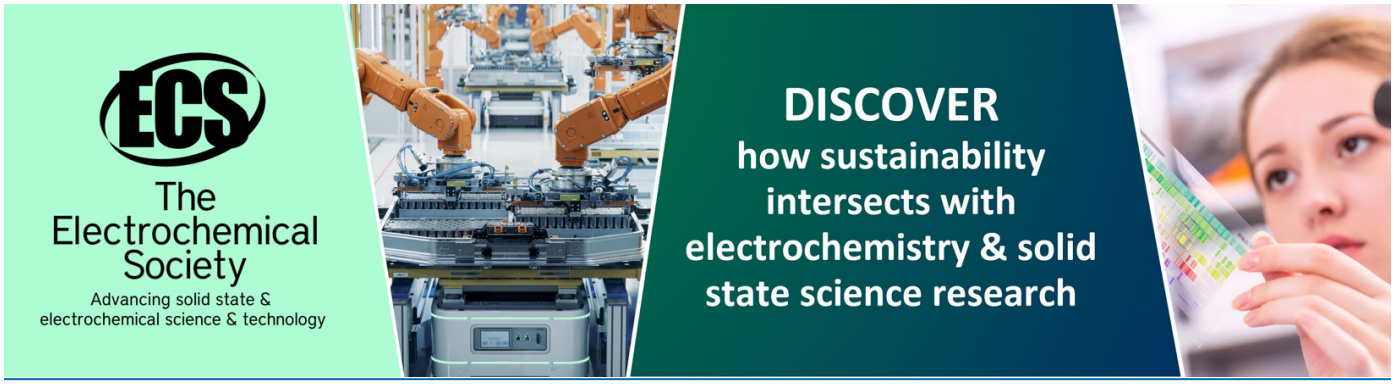

IOP Conf. Series: Materials Science and Engineering **205** (2017) 012023 doi:10.1088/1757-899X/205/1/012023

Titania with Alkaline Treated Graphitic Carbon Nitride (g-C_3N_4) to Improve Photocatalysis Properties

Wei Han Tan[1], Chen Hong Hak[1], Pichiah Saravanan[2], Kah Hon Leong[1], Lan Ching Sim[1]

[1]Department of Environmental Engineering, Faculty of Engineering and Green Technology, Universiti Tunku Abdul Rahman, Kampar, Perak, Malaysia.
[2]Department of Environmental Science and Engineering, Indian Institute of Technology, Dhanbad, India.
ch.hak117@gmail.com

Abstract. The graphitic carbon nitride (g-C_3N_4) was treated via alkaline hydrothermal treatment to change the porous structure of g-C_3N_4 to "tube-like" structure. The developed alkaline treated g-C_3N_4 (A-g-C_3N_4) was combined with P25 Degussa TiO_2 for the competent removal of methylene blue (MB). The morphological changes increased the crystallite size and pore size of g-C_3N_4, causing a decrease in the specific surface area of A-g-C_3N_4. The pure g-C_3N_4 demonstrated the best degradation efficiency among the all samples due to its high specific surface area, low band gap energy and small pore size. The combination of both A-g-C_3N_4 and g-C_3N_4 with TiO_2 did not exert significant effect on the degradation efficiency of MB owing to the low specific surface area, high band gap and large pore size. Thus concluding the degradation efficiency of organic dye is attributed predominantly to the factors of energy band gap, specific surface area and pore sizes.

1. Introduction

TiO_2 is commonly used as photocatalyst for reductive and oxidative reactions on its surface among the semiconductors. To boost the photocatalytic efficiency of TiO_2, the mass transfer limitation has to be minimized since photocatalytic reaction mainly occurs on the surface of TiO_2. The adsorption of organic pollutants on TiO_2 surface is restricted by its poor affinity towards the pollutants. Therefore, how to concentrate the target pollutants around the TiO_2 nanoparticles to enhance photocatalytic efficiency requires consideration. The TiO_2 nanoparticles may undergo aggregation due to the instability of the nanosized particle during the photocatalytic degradation process which may hamper the light incidence on the active centers and consequently reduce its catalytic activity [1,2]. TiO_2 has been highly employed for commercial purposes, due to its better photoactivity and stability under ultraviolet (UV) radiation i.e., $\lambda < 400$ nm. Though it has above mentioned advantages the major limitations are: a) It is active only under UV light and can only absorb about 5% of sunlight in the UV region [3] and b) high recombination rate of photoinduced charge carriers cause TiO_2 unable to apply efficiently [4]. Graphitic carbon nitride material (g-C_3N_4) has recently emerged as a novel photocatalyst attributed to its visible-light driven band gap (2.69 eV), high thermal and chemical stability, and facile synthesis method. However, the surface area of g-C_3N_4 is relatively small (14.3 m^2/g) [5]. It is considered that the small specific surface area of g-C_3N_4 could contribute to the slow photocatalytic reaction rate [6]. The specific surface area of g-C_3N_4 need to be increased to make g-C_3N_4 become a promising and versatile semiconductor for sunlight harvesting [7,8].

2. Preparation of g-C_3N_4 and A-g-C_3N_4

20 g of urea (R & M Marketing Essex, U.K) was dried in an oven at 80 ℃ for 1 day and then put in a muffle for 3 h at 500 ℃. The yellowish product was washed with nitric acid (0.1 M) several times and distilled water to remove any residual alkaline species. The g-C_3N_4 and 90 cm^3 of NaOH (0.10 mol dm^{-3}) solutions were mixed in Teflon-lined autoclave and subjected to hydrothermal treatment at 150 ℃ for 18 h. The solid product was then dried at 80 ℃ for 24 h and the as-obtained sample was denoted as A-g-C_3N_4.

2.1. Synthesis of g-C_3N_4/A-g-C_3N_4 hybridized TiO_2

0.15 g prepared g-C_3N_4/A-g-C_3N_4 sheet was well dispersed in distilled water ultrasonically. 4.8 g of freshly prepared P25 Degussa TiO_2 was then added into the solution and subjected to 70 ℃ for 1 h. The resulting suspension was then centrifuged and washed repeatedly with distilled water for few times and dried overnight at 60 ℃. The sample obtained by synthesized was denoted as g-C_3N_4/TiO_2 and A-g-C_3N_4/TiO_2, respectively.

2.2. Characterization

The powder X-ray diffraction (XRD, PANalytical-Empyrean) patterns were acquired with Cu Kα radiation at a scanning speed of $0.02s^{-1}$. High resolution transmission electron microscope (HRTEM, JEM-2100F, Jeol) images were obtained at 200 kV. The EDX analysis of the A-g-C_3N_4/TiO_2 was observed on a field emission scanning electron microscope (FESEM JEOL 6701-F). The Brunauer–Emmett–Teller specific surface area and pore volume of samples was determined at liquid nitrogen temperature (77 K) based on nitrogen adsorption-desorption isotherms with TriStar II 3020 (Micrometrics®, USA).

2.3. Photocatalytic degradation of organic pollutants

0.02 g of photocatalysts were immersed in a glass beaker containing 250 mL aqueous solutions for MB (5 ppm). Prior to photodegradation and to establish an adsorption-desorption equilibrium, the solutions were magnetically stirred in a dark for 1 h. A 500 W tungsten-halogen lamp was used as visible light source with filter glass to filter UV light ($\lambda < 420$nm). The dye samples were collected at regular interval, then analyzed for residual MB concentration with visible spectrophotometer (DR 6000 ™ UV-Vis spectrophotometer (Hach)) to measure the intensity of light passing through MB (λ_{max}= 664 nm).

3. HRTEM and EDX

In figure 1, it is clearly seen that TiO_2 nanoparticles were well distributed on the surface of g-C_3N_4. The surface of A-g-C_3N_4 was aggregated with nanoclusters of TiO_2 due to the nanometer effect [9]. The EDX spectrum for elemental compositions of the g-C_3N_4/TiO_2 is illustrated in figure 1b, confirming the prepared sample was a constituent of C, Ti, O and N.

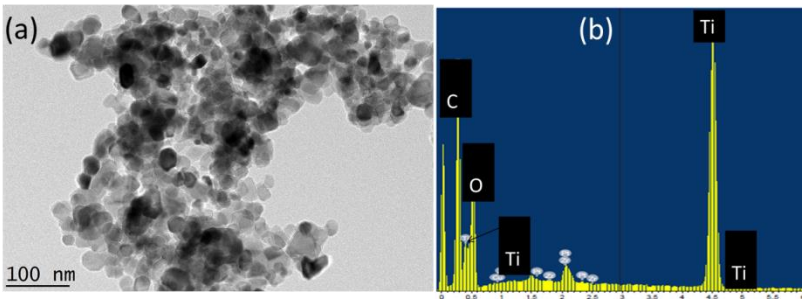

Figure 1. (a) HRTEM and (b) EDX spectrum for elemental compositions of the A-g-C_3N_4/TiO_2

4. Crystallite size and BET surface

The average crystallite sizes of TiO_2 anatase and g-C_3N_4 were calculated using Scherrer equation:

$$D = \frac{K\lambda}{\beta \cos\theta} \quad (1)$$

where K is the shape factor taken as 0.89 for calculations, λ is the wavelength of X-ray (0.154 nm), β is the full width half maximum (FWHM) for the 2θ peak, and θ is the diffraction angle. The crystallite size of TiO_2 anatase and g-C_3N_4 is listed in table 1. After incorporating both g-C_3N_4 and A-g-C_3N_4 in binary composites, it is observed that the crystallite size of TiO_2 decreased while the crystallite size of g-C_3N_4 increased. The size of TiO_2 was inhibited by the g-C_3N_4 nanosheet since TiO_2 nucleated and grew on the g-C_3N_4 surface [8]. The alkaline hydrothermal treatment of g-C_3N_4 significantly increased the crystallize size of A-g-C_3N_4 to 43.17 nm and thus, a decreasing specific surface area could occur in this sample.

Table 1: Average crystallite size for P25, A-g-C_3N_4/TiO_2, g-C_3N_4, A-g-C_3N_4 and g-C_3N_4/TiO_2

Sample	Crystallite size(nm)[a]	Crystallite size(nm)[b]
P25	32.35	-
A-g-C_3N_4/TiO_2	24.7	43.17
g-C_3N_4	-	5.27
A-g-C_3N_4	-	18.68
g-C_3N_4/TiO_2	25.26	35.04

a: TiO_2
b: g-C_3N_4

According to the International Union of Pure and Applied Chemistry (IUPAC) classification, all of the samples in figure 2 demonstrated adsorption-desorption isotherms of type III which indicating the existence of mesopores. Characteristic of type III was the heat of adsorption less than the adsorbate heat of liquification, adsorption and the interaction with the adsorbent surface is lower than the adsorbate interaction with an adsorbed layer [10]. The shape of the hysteresis loop is Type H2 when the low P/P_0 range from 0.5 to 0.8, indicating the existence of ink-bottle pores with broad bodies and narrow necks [5].

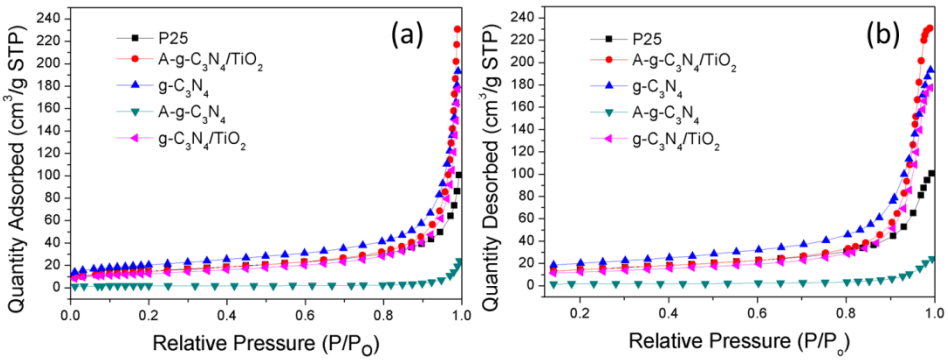

Figure 2. (a) Adsorption and (b) desorption isotherms of P25, A-g-C_3N_4/TiO_2, g-C_3N_4, A-g-C_3N_4 and g-C_3N_4/TiO_2 measured at 77 K

5. Photocatalytic Experiment

Figure 3 depicts visible-light-induced photocatalytic activity with the aid of prepared photocatalysts. The photocatalytic performance followed an order of g-C_3N_4 (62.67%) > P25 (49.47%) > A-g-C_3N_4 (47.33%) > A-g-C_3N_4/TiO_2 (46.87) > g-C_3N_4/TiO_2 (45.79%). The g-C_3N_4 showed higher photodegradation efficiency which was 62.67% compared to that of other samples, while g-C_3N_4/TiO_2 exhibited the lowest photodegradation efficiency which was 45.79% (table 2). In addition, the large specific surface area of g-C_3N_4 (71.8 m^2g^{-1}) could provide more active adsorption sites for the reactant, and thus leading to superior degradation efficiency. The photodegradation efficiency of g-C_3N_4/TiO_2

was slightly lower than that of A-g-C_3N_4/TiO_2 and A-g-C_3N_4 due to its specific area was smaller than A-g-C_3N_4/TiO_2 and its band gap was higher than A-g-C_3N_4.
Due to the large band gap and fast recombination rate of photo-generated electron-hole pairs, the other sample showed lower photodegradation efficiency than g-C_3N_4 [11]. The narrowest band gap in pure A-g-C_3N_4 did not lead to the enhancement of photocatalytic performance due to its small specific surface area, which was 6.3 $m^2 g^{-1}$. The photocatalytic activity performance was related to the specific area of the photocatalyst, the higher the specific surface area of the photocatalyst, the higher the photocatalytic activity [12]. The samples of A-g-C_3N_4/TiO_2, A-g-C_3N_4 and g-C_3N_4/TiO_2 showed an outstanding visible light harvesting properties, but their large pore sizes ranging from 230 to 270 nm and low specific surface area large contributed to the poorer photocatalytic activity compared to that of P25 TiO_2. The observed degradation data were fitted to the simple kinetic model and tabulated in table 2. The first-order reaction kinetics is expressed by equation:

$$\ln\left(\frac{C}{C_o}\right) = -kt \qquad (2)$$

where k is the first-order reaction constant, C_0 and C are the MB concentrations in solution at times 0 and t, respectively.

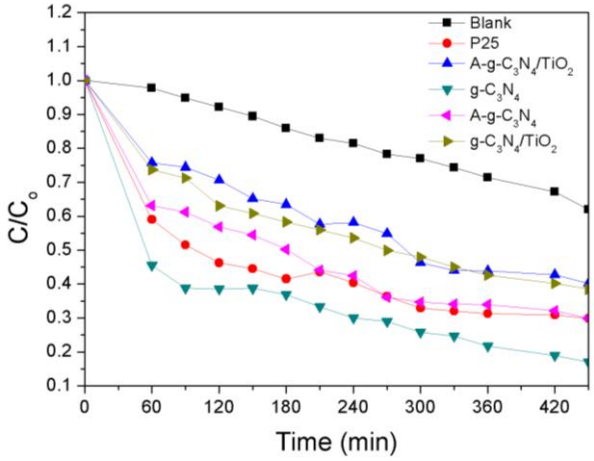

Figure 3. Photocatalytic degradation of MB as a function of reaction time

Table 2: Degradation rate of MB by P25, A-g-C_3N_4/TiO_2, g-C_3N_4, A-g-C_3N_4 and g-C_3N_4/TiO_2

Sample	Degradation Rate[a] (%)	K[b] (min^{-1})
Blank(control)	32.78	0.001
P25	49.47	0.002
A-g-C_3N_4/TiO_2	46.87	0.002
g-C_3N_4	62.67	0.003
A-g-C_3N_4	47.33	0.002
g-C_3N_4/TiO_2	45.79	0.002

[a] after reaction for 6 h
[b] apparent rate constant deduced from linear fitting of ln(C/C_0) versus reaction time

6. Conclusion

In summary, the binary composites namely A-g-C_3N_4/TiO_2 and g-C_3N_4/TiO_2 was successfully synthesized *via* a simple and facile method. The prepared binary composites displayed non appreciable changes in the photocatalytic performance compared to that of pure g-C_3N_4. This is mainly due to the decreasing specific surface area in binary nanocomposites when the titania agglomerated on the surface of both g-C_3N_4 and A-g-C_3N_4. The overetching effect caused by the non-optimized conditions of alkaline hydrothermal treatment also contributed to a trivial photocatalytic activity of A-g-C_3N_4.

Hence, the specific surface area and crystallite size played a crucial role in boosting the photocatalytic performance of photocatalysts.

References

[1] Gao B, Yap P S, Lim T M and Lim T T 2011 Adsorption-photocatalytic degradation of acid red 88 by supported TiO_2: effect of activated carbon support and aqueous anions *Chem. Eng. J.* **171(3)** 1098-1107.

[2] Mallakpour S and Nikkhoo E 2014 Surface modification of nano-TiO_2 with trimellitylimido-amino acid-based diacids for preventing aggregation of nanoparticles *Adv. Powder Technol.* **25(1)** 348-353.

[3] Dong H, Zeng G, Tang L, Fan C, Zhang C, He X and He Y 2015 An overview on limitations of TiO_2-based particles for photocatalytic degradation of organic pollutants and the corresponding countermeasures *Water Res* **79** 128-146.

[4] Bagwasi S, Niu Y, Nasir M, Tian B and Zhang J 2013 The study of visible light active bismuth modified nitrogen doped titanium dioxide photocatlysts: role of bismuth *Appl. Surf. Sci.* **264** 139-147.

[5] Hao R, Wang G, Tang H, Sun L, Xu C and Han D 2016 Template-free preparation of macro/mesoporous g-C_3N_4/TiO_2 heterojunction photocatalysts with enhanced visible light photocatalytic activity *Appl. Catal. B: Environ.* **187** 47-58.

[6] Sano T, Tsutsui S, Koike K, Hirakawa T, Teramoto Y, Negishi N and Takeuchi K 2013 Activation of graphitic carbon nitride (g-C_3N_4) by alkaline hydrothermal treatment for photocatalytic NO oxidation in gas phase *J. Mater. Chem.* A **1(21)** 6489-6496.

[7] Chen X, Wei J, Hou R, Liang Y, Xie Z, Zhu Y, Zhang X and Wang H 2016 Growth of g-C_3N_4 on mesoporous TiO_2 spheres with high photocatalytic activity under visible light irradiation *Appl. Catal. B: Environ.* **188** 342-350.

[8] Tong Z, Yang D, Xiao T, Tian Y and Jiang Z 2015 Biomimetic fabrication of g-C_3N_4/TiO_2 nanosheets with enhanced photocatalytic activity toward organic pollutant degradation *Chem. Eng. J.* **260** 117-125.

[9] Li C, Sun Z, Xue Y, Yao G and Zheng S 2016 A facile synthesis of g-C_3N_4/TiO_2 hybrid photocatalysts by sol–gel method and its enhanced photodegradation towards methylene blue under visible light *Adv. Powder Technol.* **27(2)** 330-337.

[10] Leddy N 2012 Surface area and porosity Available at: http://cma.tcd.ie/misc/Surface_area_and_porosity.pdf [Accessed 17 August 2016]

[11] Faisal M, Ismail A A, Harraz F A, Al-Sayari S A, El-Toni A M and Al-Assiri M S 2016 Synthesis of highly dispersed silver doped g-C_3N_4 nanocomposites with enhanced visible-light photocatalytic activity *Mater. Design* **98** 223-230.

[12] Li J, Liu Y, Li H and Chen C 2016 Fabrication of g-C_3N_4/TiO_2 composite photocatalyst with extended absorption wavelength range and enhanced photocatalytic performance *J. Photoch. Photobio. A* **317** 151-160.